Energetic ion loss detector on the Alcator C-Mod tokamak

D. C. Pace,[1,a)] R. S. Granetz,[2] R. Vieira,[2] A. Bader,[2] J. Bosco,[2] D. S. Darrow,[3] C. Fiore,[2]
J. Irby,[2] R. R. Parker,[2] W. Parkin,[2] M. L. Reinke,[1] J. L. Terry,[2] S. M. Wolfe,[2] S. J. Wukitch,[2]
and S. J. Zweben[3]

[1]*Oak Ridge Institute for Science and Education, Oak Ridge, Tennessee 37831, USA*
[2]*Plasma Science and Fusion Center, Massachusetts Institute of Technology, Cambridge,*
Massachusetts 02139, USA
[3]*Princeton Plasma Physics Laboratory, Princeton, New Jersey 08540, USA*

A scintillator-based energetic ion loss detector has been successfully commissioned on the Alcator C-Mod tokamak. This probe is located just below the outer midplane, where it captures ions of energies up to 2 MeV resulting from ion cyclotron resonance heating. After passing through a collimating aperture, ions impact different regions of the scintillator according to their gyroradius (energy) and pitch angle. The probe geometry and installation location are determined based on modeling of expected lost ions. The resulting probe is compact and resembles a standard plasma facing tile. Four separate fiber optic cables view different regions of the scintillator to provide phase space resolution. Evolving loss levels are measured during ion cyclotron resonance heating, including variation dependent upon individual antennae. © *2012 American Institute of Physics*. [http://dx.doi.org/10.1063/1.4731655]

I. INTRODUCTION

The tokamak concept[1] of energy production through nuclear fusion requires the magnetic confinement of fusion-produced energetic particles such that the plasma becomes self-heated. Energetic particle populations, produced by auxiliary heating and nuclear processes, are capable of driving instabilities[2] that affect plasma performance. Considerable progress in understanding energetic ion physics has been achieved,[3,4] and this will necessarily be applied to the new and unique parameter space realized in ITER.[5] The issue of energetic ion losses comes to the forefront, however, because of the potential for damage to ITER's plasma facing components. In the most extreme experimental case, energetic ion losses led to a vacuum break in TFTR.[6] Recent simulation studies of energetic ion power reaching the ITER walls under expected plasma conditions find that, while the loading due to some instabilities is within tolerance,[7] there are operating scenarios that produce a potentially damaging power flux from lost neutral beam ions.[8,9]

Scintillator-based energetic (or "fast") ion loss detectors (FILDs) are capable of measuring the pitch angle and energy of ions that reach the probe. The concept involves securing a scintillator plate within an enclosure featuring a collimating aperture, as shown in Figs. 1(a) and 1(b). Ions of sufficiently large gyroradius pass through the aperture and then impact at positions across the scintillator plate according to their pitch angle and gyroradius as depicted in the diagram of Fig. 1(c). Measured gyroradii are converted to energies given the magnetic field at the detector. FILDs have been used to measure escaping α-particles resulting from DT-fusion in TFTR,[10] and energetic ions produced by auxiliary heating methods (and lost due to various plasma instabilities or equilibrium effects) in NSTX,[11] AUG,[12] DIII-D,[13] and JET.[14] The valuable phase

space observations possible with a FILD are encouraging design studies for a reciprocating probe on ITER.[15]

Alcator C-Mod (Refs. 16 and 17) is a compact ($R = 0.68$ m and $a = 0.22$ m) and high-field ($2.3 \leq B_t \leq 8.1$ T) tokamak in which ion cyclotron resonance heating (ICRH) routinely couples 5 MW of power to the plasma. When applied to deuterium plasmas featuring a hydrogen minority fraction of order 5%, the ICRH power is capable of producing energetic protons of energy $E \leq 2$ MeV.[18] The energetic ion population is of great interest for its effects on the confined plasma in addition to possible wall damage. This kinetic population is capable of inducing global effects such as poloidal asymmetries in impurity density.[19] The absorption of ICRH energy itself is observed to be a three-dimensional problem due to the discrete location and finite extent of antennae.[20] The high magnetic field of C-Mod previously allowed for the development of charged fusion product probes.[21,22] These were successfully applied to the measurement of fusion rates and the determination of ion temperatures, but noise and sensitivity issues limited the range of operating parameters over which this was possible.[23] This paper describes the first FILD-type diagnostic system to be installed and operated on C-Mod for the explicit purpose of detecting lost energetic ions resulting from ICRH in the H-minority scenario. Simplifying design choices have been implemented, the resulting detector is measuring lost ICRH tail ions, and a series of upgrades are identified to significantly improve this system in the near future.

II. PROBE HEAD DESIGN

The FILD probe head is machined from a block of the molybdenum alloy TZM. This is the same material used to fabricate plasma facing tiles and it is chosen to reduce concern over probe heating during plasma operations. The probe head is forced to be small based on C-Mod parameters.

a)Present address: General Atomics, P. O. Box 85608, San Diego, California 92186-5608, USA. Electronic mail: pacedc@fusion.gat.com.
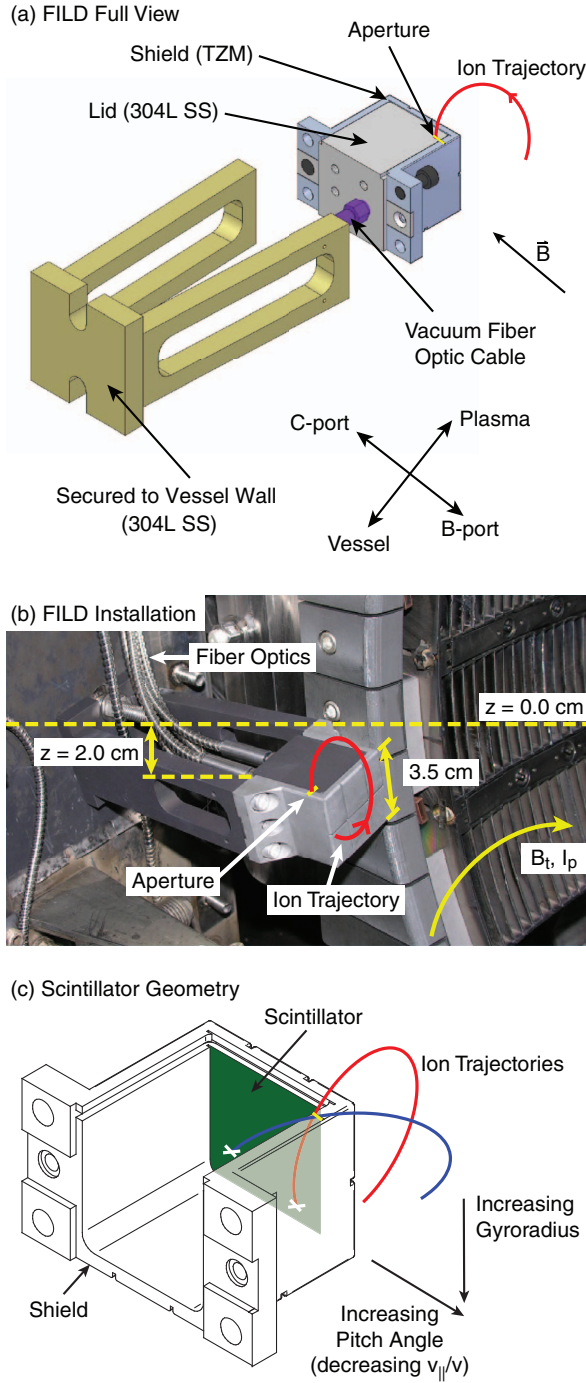
FIG. 1. (a) Schematic diagram of the FILD. (b) Photograph of the FILD as installed in C-Mod. (c) Schematic of the FILD shield demonstrating different ion strike points along the scintillator.

Approaching ions must be able to reach and pass through the aperture instead of impacting the shield. One design consideration is the transit distance, ΔL, of energetic ions in a single gyroperiod, T_{ci}. This distance must be larger than the respective dimension along the probe head, or the ion will strike the shield instead of reaching the scintillator as shown in Fig. 2(a). This distance is given by

$$\Delta L = v_{\parallel} T_{ci} = 8.328 \times 10^{-16} \frac{\mu v_{\parallel}}{v Z B} \sqrt{\frac{2E}{m}}, \qquad (1)$$
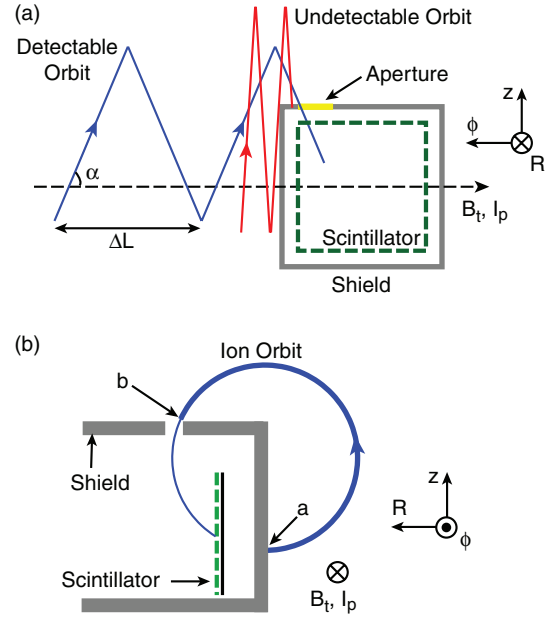

FIG. 2. Depictions of the transit distance, ΔL, with respect to (a) reaching the aperture, and (b) the portion of a gyroperiod that sets the distance.

where ΔL is in meters, $\mu = m/m_p$ is the ion mass in units of proton masses, Z is the charge state, B (T) is the local magnetic field, E (keV) is the ion energy, and m (kg) is the ion mass. The pitch of the ion is given as $v_{\parallel}/v = \cos(\alpha)$, where $v_{\parallel}$ is the ion velocity along the magnetic field, v is the total velocity, and α is the pitch angle with respect to the magnetic field. The high magnetic field of C-Mod requires a smaller probe head compared to other tokamaks. For example, considering common ion properties of $E = 80$ keV and $v_{\parallel}/v = 0.2$ for a proton in C-Mod and a deuteron in DIII-D,[24, 25] $\Delta L = 1.3$ cm in C-Mod compared to $\Delta L = 4.9$ cm in DIII-D. The distance traveled by an ion before it either hits the shield or passes through the aperture is actually shorter than ΔL. This occurs because the ion completes only some fraction of a gyro-orbit between the time it passes the edge of the shield and reaches the vertical position of the aperture. Figure 2(b) demonstrates this process in which the actual distance traveled from shield edge to aperture is the fraction of the gyro-orbit covered between points a and b. The lower limit of these values is a few millimeters in C-Mod. A rectangular shape is chosen to minimize the distance (along the toroidal coordinate, ϕ) between the shield edge and the aperture. As a result, the FILD is capable of measuring lost ions with pitch angles $\lesssim 85°$ (full details given in Sec. V).

Figure 3(a) is a photograph of the FILD probe head in which the aperture is seen to extend nearly to the edge of the shield. The aperture is 5.90 mm in length (setting the pitch angle resolution) and 0.57 mm in width (setting the gyroradius/energy resolution). The scintillator is coated onto a 0.38 mm thick stainless steel shim that fits into narrow grooves cut within the shield as shown in Fig. 3(b). This secures the scintillator in place, while also providing poor thermal contact to the plasma facing shield. The scintillator material is Maui 535 (M535) from Lightscape Materials, Inc.[26] The chemical formula of this material is $SrGa_2S_4$:Eu, and it was formerly available under the product name TG-Green. A
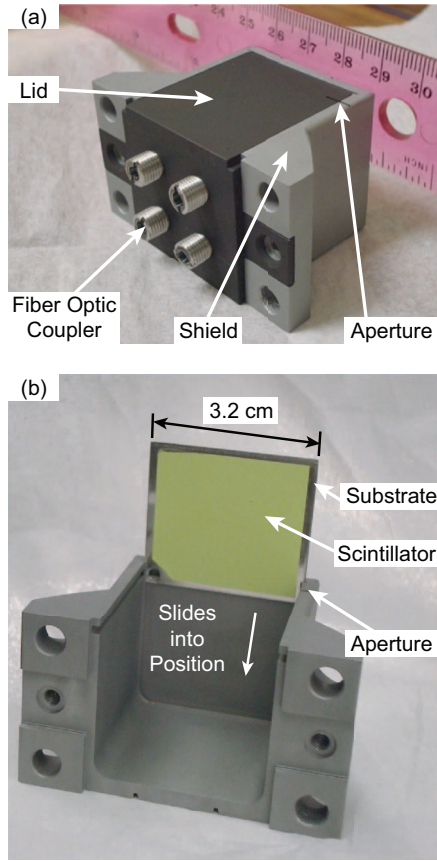
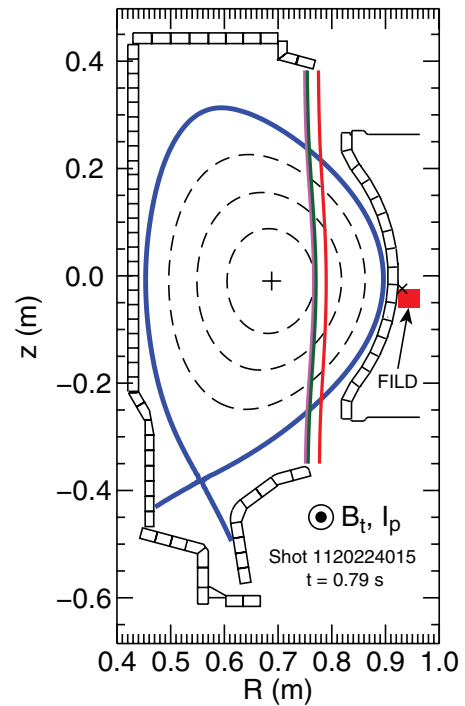FIG. 3. Photographs of the FILD probe head showing (a) the fiber optic couplers and (b) scintillator.

FIG. 4. Magnetic equilibrium from shot 1120224015 at $t = 0.79$ s. The FILD detector is shown, and the $\times$-symbol indicates the position of the aperture. The three vertical lines represent resonance locations of the injected ion cyclotron resonance heating power (80.0, 80.5, and 78.0 MHz from smaller to larger major radius, where the 80.0 and 80.5 MHz resonances are separated by ≈ 1 cm and may appear to be a single resonance).

thorough survey of different scintillator candidates identified this option as the most suitable to the vacuum, thermal loading, and radiation environments of tokamaks.[27] Peak emission occurs at a wavelength of $\lambda = 534$ nm and the decay time is $\Delta t = 490$ ns. The fast response capability of the scintillator allows for the resolution of fluctuations up to 1 MHz, which is sufficient to observe coherent losses that may be generated at the frequencies of most energetic ion-related Alfvénic activity[28] in C-Mod.

III. INSTALLATION POSITION

The installation location of the FILD sets the primary limitations on ion detection. It is not presently possible to install the detector on a reciprocating arm, primarily due to the need for a nearly 2 m long boom capable of passing through the cryostat and vacuum vessel while supporting optical elements (this same limitation prevented the direct installation of a TFTR loss detector[29] on C-Mod). A schematic for the fixed probe is shown in Fig. 1(a). A stainless steel mounting bracket is secured to the vessel wall, with the probe head attached. This bracket is known to be capable of withstanding forces encountered during experimental operations because it is the same design that secures fast-response magnetic probes, which have themselves evolved from the initial magnetic probes installation.[30] The installed detector is pictured in Fig. 1(b). The position of the FILD along the major radius coordinate, R, is chosen to ensure that energetic ions reach it

while also keeping the entire detector radially behind plasma limiting surfaces. Figure 4 shows an EFIT (Ref. 31) magnetic equilibrium from shot 1120224015 which features $B_t = 6.0$ T and plasma current $I_p = 0.9$ MA. A labeled rectangle represents the FILD probe head, and the $\times$-symbol on top of that rectangle marks the location of the collimating aperture. The shape of a typical outboard limiter is plotted for reference, and the FILD aperture is 3 cm behind (i.e., at larger major radius) the innermost limiter surface. The FILD is able to collect energetic ions because there is sufficient toroidal separation between it and the limiting surfaces, as shown in the following ion orbit study.

Qualification of the FILD's ability to capture lost ions is performed by reviewing energetic ion trajectories in a variety of relevant equilibria. Orbits are calculated using an updated version of the Lorentz force code ORBIT (Ref. 32) that has been modified to read C-Mod equilibria. An example of this modeling is given in Fig. 5. Orbits for two energetic protons are shown with respect to the limiter boundary at $R = 0.9$ m. Both orbits are calculated with a pitch of $v_\parallel/v = 0.5$. Figure 5 shows that a toroidal clearance of $\Delta\phi = 45°$ is necessary for these ions to reach the FILD instead of hitting the limiter. A wide survey of relevant orbits and plasma parameters finds that a toroidal clearance of $\Delta\phi = 40°$ provides a sufficient range of expected detection. Experimentally realized conditions are more favorable, however, because the limiter is not toroidally continuous and other segments are positioned at larger major radii.

After identifying the necessary toroidal clearance, a toroidal installation position is identified. This position is
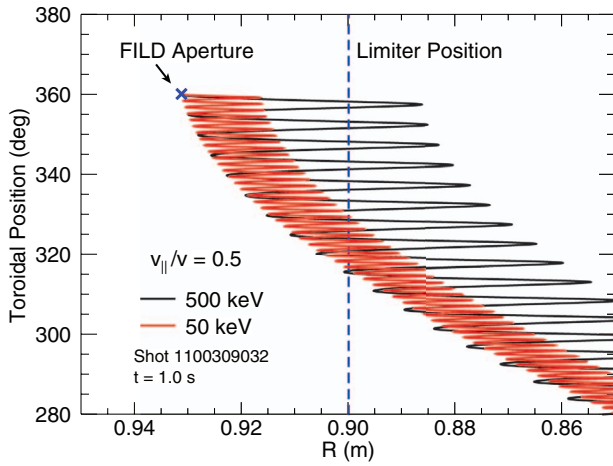
FIG. 5. Proton trajectories in the $R\phi$-plane. The $\times$-symbol represents the FILD aperture and the dashed vertical line indicates the limiting surface at $R = 0.9$ m.

illustrated by the tokamak top-view of Fig. 6. The toroidal layout map includes the three ICRH antennae (RF), the lower hybrid launcher (LH), and the three limiters (solid rectangles). The FILD is installed adjacent to the LH-launcher with its aperture directed towards B-port. There is $\smile$40° of toroidal distance between the FILD and the nearest limiter. That limiter, the AB-split limiter, consists of two separate poloidal segments above and below the midplane. Technical limitations related to the path of the output fiber optic cables prevent installation at other suitable locations such as the limiter between ports G and H. Given that the toroidal installation position is fixed, small adjustments to the radial position are being considered. Moving the FILD 5 mm radially closer to the plasma has the potential to noticeably increase signal levels, though doing so requires additional consideration for heat loads on the shield and lid.

IV. SIGNAL COLLECTION

Scintillator light is collected by four discrete fiber optic cables as indicated in Figs. 1(a), 1(b), and 3(a). Each fiber collects any emitted light within the solid angle defined by
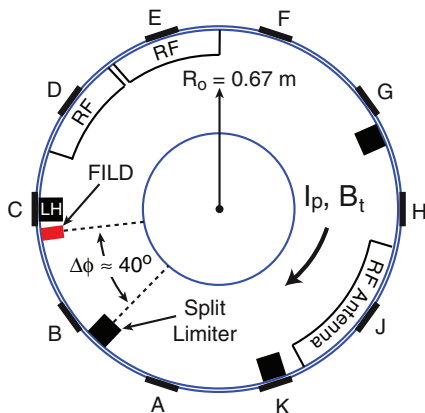

FIG. 6. Top view of the tokamak indicating the ports (A-K, there is no I-port) and the toroidal layout along the outer wall. The toroidal separation, $\Delta\phi$, between the FILD and the nearest limiter is shown.

its numerical aperture. The four cables are 400 μm diameter vacuum-compatible high-hydroxyl content silica with numerical aperture of 0.22 manufactured by FiberTech-RoMack.[33] Procedures for incorporating fiber optic cables in-vacuum at C-Mod have been developed based on experience with multiple diagnostics, including the discrete channels of the gas puff imaging system.[34] Prior to assembly, the manufacturer sends the fiberglass sleeves and stainless steel jacketing for cleaning by the Vacuum Group. These materials are then returned to the manufacturer for final assembly. At the probe head, the SMA905 terminations of the cables connect to custom fittings as shown in Fig. 3(a). The cables are secured to the vessel wall along their path to a flange at the bottom of the vessel. The vacuum interface is a 3-3/8″ CONFLAT flange with four individual SMA905 fiber optic feedthroughs. Outside of the vacuum vessel, a set of 10 m long fiber optic cables (same specification as the vacuum cable, but without the need for special cleaning) travel through the tokamak cell and connect to photomultipliers (Hamamatsu[35] model H10721-210). These photomultipliers (PMTs) feature peak sensitivity at a wavelength of 400 nm and operate with a bandwidth of 1.7 GHz at maximum gain. Outputs from the PMTs are passed to a transimpedance amplifier that connects to a D-tAcq digitizer.[36] The PMTs are placed inside magnetic shields (0.062″ thick CO-NETIC AA alloy custom manufactured by Magnetic Shield Corporation[37]) and packed, along with the amplifier and control electronics, into an electromagnetic shield box (custom size version of model R58060 from Compac Development Corporation[38]). FILD signals are digitized at 2 MHz to take advantage of the full time response of the scintillator. After each plasma discharge, data are transferred from the on-board memory of the digitizer to database storage under MDSplus (Refs. 39 and 40) control. The PMT gain is controlled through a standard networked terminal and the digitizer settings, including the trigger, are controlled through an MDSplus interface.

V. ANALYSIS AND INITIAL RESULTS

A map of the measurable ion phase space across the scintillator is shown in Fig. 7. This is calculated by the NLSDET-SIM (Ref. 29) code, which traces helical trajectories based on the geometry of the probe head and the local magnetic field. For each gyroradius/pitch angle pair, the code begins the orbit from a variable position within the volume defined to represent the aperture. The displayed strike map is calculated from 2×10^6 attempted trajectories for each pair. The calculation is a simple helix trajectory centered on the user-defined vector representing the magnetic field (determined from the equilibrium), i.e., this is a calculation of geometric properties, not electromagnetic forces. As a result, the grid is output in units of pitch angle and gyroradius according to the average strike position of all the helices that reached the scintillator plane. Some of these trajectories intersect the probe head instead of the scintillator and do not contribute to the determination of the grid point. Figure 7(a) displays a strike map from shot 1120224022 ($B_t = 5.3$ T and $I_p = 1.0$ MA) using the magnetic equilibrium at $t = 1.2$ s. Four circles on the map represent the observed phase spaces of the PMT channels based
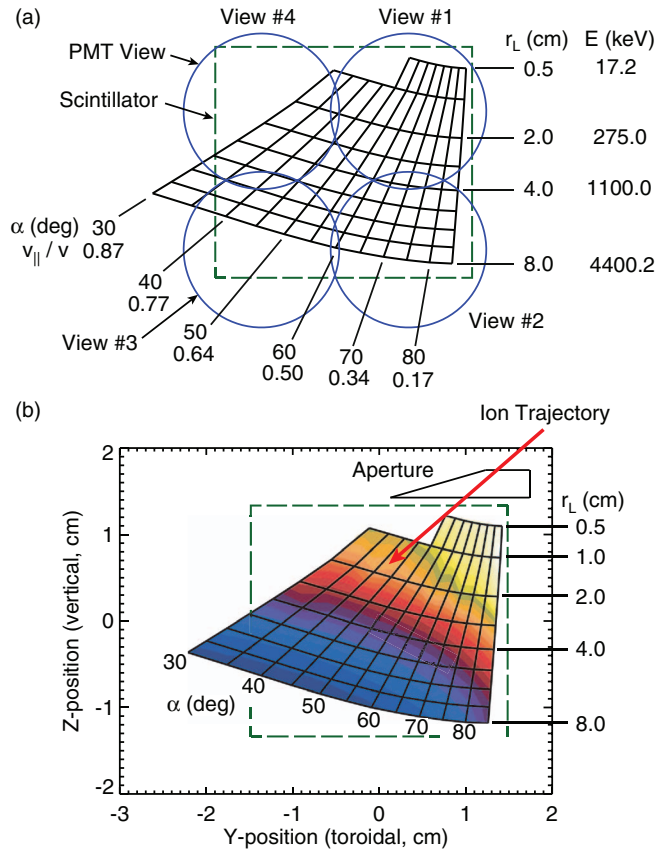
FIG. 7. Strike map based on the magnetic equilibrium in shot 1120224022 at $t = 1.2$ s. (a) Phase space viewed by each PMT channel. (b) Color contour indicating the number of particles that reach the scintillator to define a grid point. Up to 55% of the test orbits reach the scintillator along $r_L = 0.5$ cm, and that value drops to 17% across most of the $r_L = 4.0$ cm line.
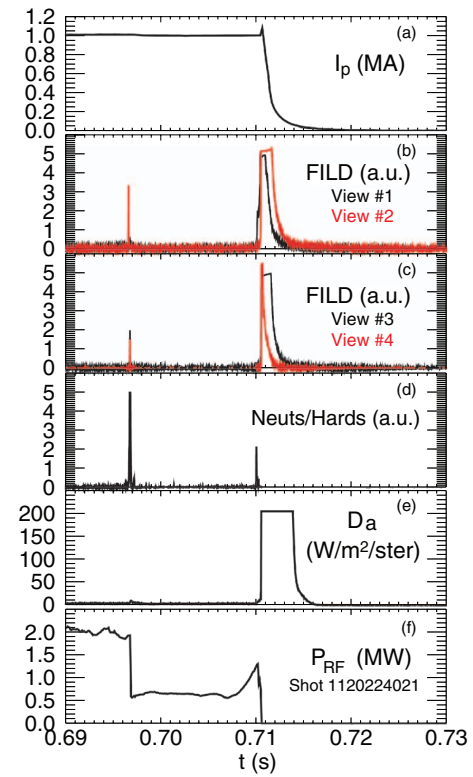

FIG. 8. Plasma evolution over a disruption in shot 1120224021: (a) plasma current, (b) FILD signal from views #1 and #2, (c) FILD signals from views #3 and #4, (d) combined neutrons and hard x-rays, (e) D_α emission, and (f) injected ICRH power.

on a bench calibration of each fiber optic view. These views are numbered 1–4 and, while their physical views are fixed, the sampled phase space depends on the magnetic field and plasma current. The same map is displayed in an alternative manner in Fig. 7(b) to highlight the diagnostic weighting in this case. The phase space position with the largest number of test orbits reaching the scintillator, 55%, occurs at $r_L = 0.5$ cm and $\alpha = 85°$. This value decreases to 17% across most of the $r_L = 4.0$ cm line. The color contour may be interpreted as the expected relative signal given an isotropic distribution of energetic ions reaching the detector. Phase space weighting is not typically considered in FILD analyses, though it is vital in other areas of energetic ion measurement.[41–43] It should be expected that understanding the weighting over phase space will become more important as FILD measurements are more regularly compared to advanced simulations.[44]

Most of the FILDs in operation at other tokamaks use an optics train to split scintillator light between a slow-sampling camera and fast-sampling PMTs. The benefit of the camera acquisition is that it provides high spatial resolution across the scintillator. Even with acquisition rates below 1 kHz, camera data are useful for confirming the accuracy of strike maps based on alignment between the grid and stripes produced by neutral beam prompt losses.[45, 46] The C-Mod installation does not allow for the necessary optics to transmit the en-

tire scintillator surface outside of the vessel, and this initial probe design is limited to four fiber optic views. Commissioning of the FILD, therefore, includes operation during Ohmic plasma experiments in order to determine its typical response to scrape-off layer (SOL) plasma light and hard x-rays. Stray light levels are investigated by comparing FILD signals to D_α measurements[47] that are dominated by light emission from the SOL. The contribution from SOL light is found to be insignificant during normal operation, though saturated signals will occasionally result from the incredible brightness produced by disruptions. It may be possible to reduce stray light contributions further by placing a spectral filter in front of the PMTs, and this will be investigated in the future [a suitable component with 40 nm bandwidth and center wavelength of 530 nm is available from Hamamatsu (part number A10033-01)]. Figure 8 illustrates both hard x-ray and disruption behavior. The disruption occurs at $t \approx 0.71$ s as indicated by the brief spike in plasma current shown in Fig. 8(a). The FILD signals from views 1 and 2 are plotted in Fig. 8(b), while the signals from views 3 and 4 are shown in Fig. 8(c). The FILD traces remain at zero level except during hard x-ray emission (indicated by the trace in pane (d), which represents the combined contribution of neutrons and hard x-rays), and the increase in SOL light following the disruption [indicated in the D_α trace of panel (e)]. The injected ICRH power is shown in Fig. 8(f), and the resulting energetic ion distribution is expected to be responsible for the small signal in FILD view #1 immediately prior to the x-ray burst at $t \approx 0.71$. The role of
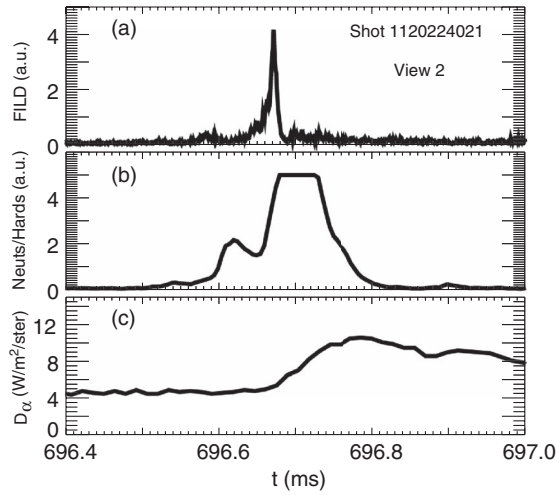
FIG. 9. Narrow time range view centered on the early hard x-ray burst from Fig. 8. (a) FILD signal from view #2, (b) combined neutrons and hard x-ray signal, and (c) D_α light emission.

FIG. 10. Discharge evolution from shot 1120224015. (a) FILD view #1, (b) injected ICRH power, P_{RF}, and central electron temperature, $T_e(0)$, (c) neutron rate and line-averaged density, $\bar{n}_e$, and (d) D_α light.

disruptions in generating energetic ion losses is an ongoing investigation.

Figure 9 presents a narrow time range view of the early hard x-ray burst occurring at $t \approx 0.697$ s in Fig. 8. Figure 9(a) is the FILD signal, which is seen to correlate with the combined neutron and hard x-ray signal shown in Fig. 9(b). The front face thickness of the FILD TZM shield is 0.32 cm, resulting in an x-ray energy requirement of $E_{\text{x-ray}} > 200$ keV for penetration. The FILD signal exhibits similar evolution compared to the hard x-ray signal, aside from the saturation. The FILD is intended for operation during lower hybrid current drive experiments.[48] In those experiments there will rarely be an energetic ion population (only in cases of simultaneous ICRH input), but the FILD's ability to detect hard x-rays and its proximity to the lower hybrid launcher may prove useful in investigating new theories concerning energetic electron generation near lower hybrid grills.[49] The D_α trace in Fig. 9(c) is shown to demonstrate that the FILD signals do not correlate with edge light outside of disruptions.

An example of measured energetic ion losses is shown in Fig. 10(a) for view #1 during discharge 1120224015 ($B_t = 6.0$ T and $I_p = 0.9$ MA). The FILD signal grows quickly following ICRH turn-on [Fig. 10(b)] at $t = 0.55$ s, but it remains at a steady value for approximately the first 200 ms of injected ICRH power. At $t \approx 0.75$ s, the FILD signal begins increasing to its peak value. The ICRH power is steady over this time period and the electron temperature (Fig. 10(b), measured by a grating polychrometer[50]) decreases slowly. Corresponding to this behavior, Fig. 10(c) shows a steadily declining neutron rate (from the detection system[51]), though this decrease seems likely to result from the increasing density (line-integrated measurement from a two-color interferometer[52]) also shown. It is theorized that the loss signal indicates a change in the ICRH tail ion distribution. A compact neutral particle analyzer array (CNPA; Ref. 53) will measure the confined ICRH tail ion distribution for comparison in future experiments (it was unavailable for this experiment).

During the later portion of this discharge, $t > 1.0$ s, each ICRH antenna is fired individually to investigate any
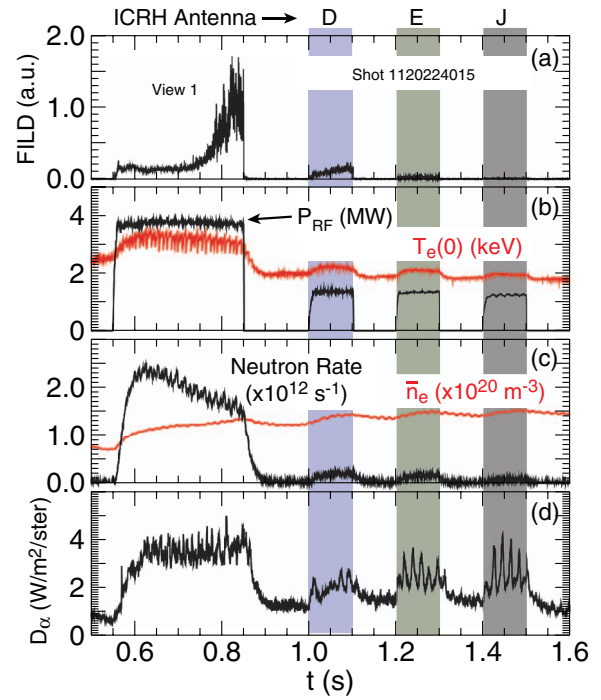
particular loss dependence. The C-Mod antennae are identified according to their port of installation. There are two-strap antennae at ports D and E, and a four-strap antenna at port J (Fig. 6). While the confined energetic ion distribution should quickly become axisymmetric during the use of a single antenna, effects near the antenna can also produce energetic ions, e.g., the FILD at DIII-D recently observed acceleration of ions in the SOL originating near a single fast wave antenna.[54] At C-Mod, the J-antenna is of an advanced and unique field-aligned design that is expected to reduce parasitic edge losses, resulting in decreased impurity generation and improved performance.[55] Figure 10 shows that the FILD signal varies according to which antenna injects power into the plasma. Significant loss signals are observed for D-antenna, along with a very small response to E-antenna, but zero response to J-antenna. While this may be consistent with the J-antenna design goals, further studies with varying plasma parameters are necessary to confirm any relation. The D_α signals in Fig. 10(d) display an opposite response, with the largest bursty features corresponding to use of J-antenna. This is another example of the FILD signal demonstrating insensitivity to stray light from the SOL.

The present phase space resolution of the FILD, while limited, is capable of contributing useful information to experiments. For example, during an experiment concerning plasma/wall interactions, low plasma current shots are used to increase energetic ion banana widths and encourage losses to the wall. FILD signals are largest from within view #1, and an ion orbit ($E = 250$ keV and $v_\parallel/v = 0.5$) based on the center of that phase space view is plotted from shot 1120224034 ($B_t = 5.4$ T and $I_p = 0.6$ MA) at $t = 0.73$ s in Fig. 11. This discharge features an upper single null plasma shape with standard magnetic field direction. Plasmas featuring such
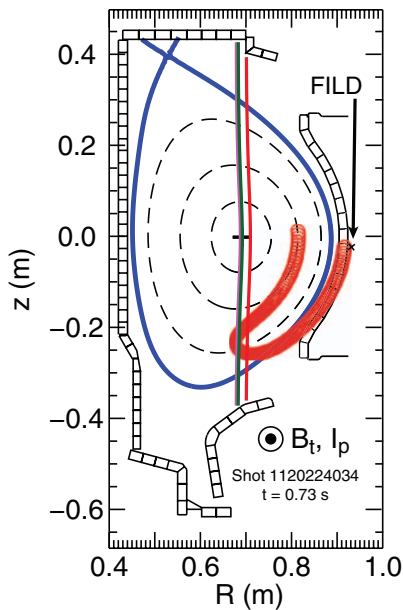
FIG. 11. Magnetic equilibrium from shot 1120224034. The three nearly vertical lines represent the ICRH resonances, the aperture of the FILD is indicated by the ×-symbol, and an energetic ion orbit intersecting the aperture has properties $E = 250$ keV and $v_\parallel/v = 0.5$.

unfavorable ∇B-drift direction are commonly run at C-Mod due to their ability to produce the improved confinement mode referred to as I-mode.[56] Since the magnetic field and plasma current remain in the standard direction, however, the FILD remains capable of capturing energetic ion orbits. The resulting banana orbit from this case has a bounce point that overlaps with the resonance layers of the D- and E-antennae. This suggests that ICRH tail ions of energy $E > 250$ keV are readily lost to the wall, with many of them striking limiting surfaces at other toroidal locations.

VI. SUMMARY

A fast ion loss detector (FILD) is installed and presently operating on the Alcator C-Mod tokamak. Interesting fast ion loss behavior has been measured during the commissioning of this diagnostic, including increased signals from a specific ICRH antenna. Future results will be applied to the interpretation of ICRH tail ion distributions measured by a neutral particle analyzer. Optimal utility of the FILD will be achieved by increasing the number of scintillator views to obtain more phase space resolution. The FILD is compact and similar to standard plasma facing tiles in both scale and material. This represents an advancement in design since future wall-integrated detectors have the potential to allow the creation of FILD arrays that provide increased phase space coverage by collecting lost ions across a greater number of toroidal and poloidal positions. Energetic ion losses are known to occur with toroidal and poloidal wall-strike dependencies due to propagating modes,[57] and simulations predict similar effects in ITER resulting from assorted magnetic symmetry-breakings.[8] While present FILD designs do not scale well, in terms of cost and port space, to arrays consisting of more than a few probes, a wall-integrated solution could alleviate those issues.

[1] J. Wesson, *Tokamaks*, 4th ed., International Series of Monographs on Physics Vol. 149 (Oxford Science, 2011).

[2] W. W. Heidbrink, Phys. Plasmas **15**, 055501 (2008).

[3] W. Heidbrink and G. Sadler, Nucl. Fusion **34**, 535 (1994).

[4] B. N. Breizman and S. E. Sharapov, Plasma Phys. Controlled Fusion **53**, 054001 (2011).

[5] A. Fasoli, C. Gormenzano, H. Berk, B. Breizman, S. Briguglio, D. Darrow, N. Gorelenkov, W. Heidbrink, A. Jaun, S. Konovalov, R. Nazikian, J.-M. Noterdaeme, S. Sharapov, K. Shinohara, D. Testa, K. Tobita, Y. Todo, G. Vlad, and F. Zonca, Nucl. Fusion **47**, S264 (2007).

[6] D. S. Darrow, S. J. Zweben, S. Batha, R. V. Budny, C. E. Bush, Z. Chang, C. Z. Cheng, H. H. Duong, J. Fang, N. J. Fisch, R. Fischer, E. D. Fredrickson, G. Y. Fu, R. F. Heeter, W. W. Heidbrink, H. W. Herrmann, M. C. Herrmann, K. Hill, E. F. Jaeger, R. James, R. Majeski, S. S. Medley, M. Murakami, M. Petrov, C. K. Phillips, M. H. Redi, E. Ruskov, D. A. Spong, E. J. Strait, G. Taylor, R. B. White, J. R. Wilson, K.-L. Wong, and M. C. Zarnstorff, Phys. Plasmas **3**, 1875 (1996).

[7] T. Kurki-Suonio, O. Asunta, E. Hirvijoki, T. Koskela, A. Snicker, T. Hauff, F. Jenko, E. Poli, and S. Sipil, Nucl. Fusion **51**, 083041 (2011).

[8] K. Shinohara, T. Kurki-Suonio, D. Spong, O. Asunta, K. Tani, E. Strumberger, S. Briguglio, T. Koskela, G. Vlad, S. Günter, G. Kramer, S. Putvinski, K. Hamamatsu, and ITPA Topical Group on Energetic Particles, Nucl. Fusion **51**, 063028 (2011).

[9] K. Tani, K. Shinohara, T. Oikawa, H. Tsutsui, S. Miyamoto, Y. Kusama, and T. Sugie, Nucl. Fusion **52**, 013012 (2012).

[10] D. S. Darrow, H. W. Herrmann, D. W. Johnson, R. J. Marsala, R. W. Palladino, S. J. Zweben, and M. Tuszewski, Rev. Sci. Instrum. **66**, 476 (1995).

[11] D. S. Darrow, Rev. Sci. Instrum. **79**, 023502 (2008).

[12] M. García-Muñoz, H.-U. Fahrbach, H. Zohm, and ASDEX Upgrade Team, Rev. Sci. Instrum. **80**, 053503 (2009).

[13] R. K. Fisher, D. C. Pace, M. García-Muñoz, W. W. Heidbrink, C. M. Muscatello, M. A. Van Zeeland, and Y. B. Zhu, Rev. Sci. Instrum. **81**, 10D307 (2010).

[14] S. Baeumel, A. Werner, R. Semler, S. Mukherjee, D. S. Darrow, R. Ellis, F. E. Cecil, L. Pedrick, H. Altmann, V. Kiptily, and J. Gafert (JET-EFDA Contributors), Rev. Sci. Instrum. **75**, 3563 (2004).

[15] E. Veshchev, L. Bertalot, S. Putvinski, M. García-Muñoz, S. Lisgo, C. Pitcher, R. Pitts, V. Udintsev, and M. Walsh, Fusion Sci. Technol. **61**, 172 (2012).

[16] E. Marmar and Alcator C-Mod Group, Fusion Sci. Technol. **51**, 261 (2007).

[17] E. Marmar, A. Bader, M. Bakhtiari, H. Barnard, W. Beck, I. Bespamyatnov, A. Binus, P. Bonoli, B. Bose, M. Bitter, I. Cziegler, G. Dekow, A. Dominguez, B. Duval, E. Edlund, D. Ernst, M. Ferrara, C. Fiore, T. Fredian, A. Graf, R. Granetz, M. Greenwald, O. Grulke, D. Gwinn, S. Harrison, R. Harvey, T. Hender, J. Hosea, K. Hill, N. Howard, D. Howell, A. Hubbard, J. Hughes, I. Hutchinson, A. Ince-Cushman, J. Irby, V. Izzo, A. Kanojia, C. Kessel, J. Ko, P. Koert, B. LaBombard, C. Lau, L. Lin, Y. Lin, B. Lipschultz, J. Liptac, Y. Ma, K. Marr, M. May, M. Mc-Dermott, O. Meneghini, D. Mikkelsen, R. Ochoukov, R. Parker, C. Phillips, P. Phillips, Y. Podpaly, M. Porkolab, M. Reinke, J. Rice, W. Rowan, S. Scott, A. Schmidt, J. Sears, S. Shiraiwa, A. Sips, N. Smick, J. Snipes, J. Stillerman, Y. Takase, D. Terry, J. Terry, N. Tsujii, E. Valeo, R. Vieira,

G. Wallace, D. Whyte, J. Wilson, S. Wolfe, G. Wright, J. Wright, S. Wukitch, G. Wurden, P. Xu, K. Zhurovich, J. Zaks, and S. Zweben, Nucl. Fusion **49**, 104014 (2009).

[18] A. Bader, P. Bonoli, R. Granetz, R. Harvey, E. Jaeger, R. Parker, and S. Wukitch, "ICRF minority-heated fast-ion distributions on the Alcator C-Mod: Experiment and simulation," Paper O-27, the *12th IAEA Technical Meeting on Energetic Particles in Magnetic Confinement Systems, Austin, Texas, September 7–10* (2011).

[19] M. L. Reinke, I. H. Hutchinson, J. E. Rice, N. T. Howard, A. Bader, S. Wukitch, Y. Lin, D. C. Pace, A. Hubbard, J. W. Hughes, and Y. Podpaly, Plasma Phys. Controlled Fusion **54**, 045004 (2012).

[20] N. Tsujii, M. Porkolab, P. T. Bonoli, Y. Lin, J. C. Wright, S. J. Wukitch, E. F. Jaeger, and R. W. Harvey, AIP Conf. Proc. **1406**, 293 (2011).

[21] R. L. Boivin, C. Kurz, D. H. Lo, C. L. Fiore, R. Granetz, and R. D. Petrasso, Rev. Sci. Instrum. **63**, 4533 (1992).

[22] D. H. Lo, R. L. Boivin, and R. D. Petrasso, Rev. Sci. Instrum. **66**, 345 (1995).

[23] D. H. C. Lo, "Charged fusion product diagnostic on the Alcator C-Mod tokamak," Ph.D. dissertation (Massachusetts Institute of Technology, 1996), also published as PSFC Report PFC/RR-96-7.

[24] J. Luxon, Nucl. Fusion **42**, 614 (2002).

[25] C. Greenfield and DIII-D Team, Nucl. Fusion **51**, 094009 (2011).

[26] See http://www.lightscapematerials.com/02_pdfs/M535.pdf for the properties of the Maui 535 scintillator material.

[27] M. García-Muñoz, "Fast response scintillator based detector for MHD induced energetic ion losses in ASDEX upgrade," Ph.D. dissertation, (Ludwig-Maximilians-Universität München, 2006).

[28] J. A. Snipes, N. Basse, C. Boswell, E. Edlund, A. Fasoli, N. N. Gorelenkov, R. S. Granetz, L. Lin, Y. Lin, R. Parker, M. Porkolab, J. Sears, S. Sharapov, V. Tang, and S. Wukitch, Phys. Plasmas **12**, 056102 (2005).

[29] S. Zweben, R. Boivin, M. Diesso, S. Hayes, H. Hendel, H. Park, and J. Strachan, Nucl. Fusion **30**, 1551 (1990).

[30] R. S. Granetz, I. H. Hutchinson, J. Gerolamo, W. Pina, and C. Tsui, Rev. Sci. Instrum. **61**, 2967 (1990).

[31] L. Lao, H. S. John, R. Stambaugh, A. Kellman, and W. Pfeiffer, Nucl. Fusion **25**, 1611 (1985).

[32] J. Felt, C. W. Barnes, R. E. Chrien, S. A. Cohen, W. W. Heidbrink, D. Manos, and S. Zweben, Rev. Sci. Instrum. **61**, 3262 (1990).

[33] See www.romackfiberoptics.com for information concerning the fiber optics.

[34] S. J. Zweben, D. P. Stotler, J. L. Terry, B. LaBombard, M. Greenwald, M. Muterspaugh, C. S. Pitcher, K. Hallatschek, R. J. Maqueda, B. Rogers, J. L. Lowrance, V. J. Mastrocola, and G. F. Renda (Alcator C-Mod Group), Phys. Plasmas **9**, 1981 (2002).

[35] See http://sales.hamamatsu.com for information concerning Hamamatsu products.

[36] See http://www.d-tacq.com/products.shtml for information concerning D-tAcq products. The digitizer is model number ACQ216CPCI-16-50-M2-1024M-RTMDDS.

[37] See http://magnetic-shield.com for information concerning Magnetic Shield Corporation products.

[38] See http://www.compac-rf.com for information concerning Compac Development Corporation products.

[39] J. A. Stillerman, T. W. Fredian, K. Klare, and G. Manduchi, Rev. Sci. Instrum. **68**, 939 (1997).

[40] G. Manduchi, T. Fredian, and J. Stillerman, "MDSplus evolution continues," Fusion Eng. Des. (in press).

[41] W. W. Heidbrink, Y. Luo, K. H. Burrell, R. W. Harvey, R. I. Pinsker, and E. Ruskov, Plasma Phys. Controlled Fusion **49**, 1457 (2007).

[42] C. Muscatello, R. Harvey, W. Heidbrink, Y. Kolesnichenko, V. Lutsenko, M. V. Zeeland, and Y. Yakovenko, "Using velocity-space resolution to determine the mechanism of fast-ion transport on DIII-D", Paper I-6, the *12th IAEA Technical Meeting on Energetic Particles in Magnetic Confinement Systems, Austin, Texas, September 7–10* (2011).

[43] M. Salewski, S. Nielsen, H. Bindslev, V. Furtula, N. Gorelenkov, S. Korsholm, F. Leipold, F. Meo, P. Michelsen, D. Moseev, and M. Stejner, Nucl. Fusion **51**, 083014 (2011).

[44] M. A. Van Zeeland, W. W. Heidbrink, R. K. Fisher, M. García-Muñoz, G. J. Kramer, D. C. Pace, R. B. White, S. Aekaeslompolo, M. E. Austin, J. E. Boom, I. G. J. Classen, S. da Graça, B. Geiger, M. Gorelenkova, N. N. Gorelenkov, A. W. Hyatt, N. Luhmann, M. Maraschek, G. R. McKee, R. A. Moyer, C. M. Muscatello, R. Nazikian, H. Park, S. Sharapov, W. Suttrop, G. Tardini, B. J. Tobias, Y. B. Zhu, DIII-D, and A. U. Teams, Phys. Plasmas **18**, 056114 (2011).

[45] D. C. Pace, R. K. Fisher, M. García-Muñoz, D. S. Darrow, W. W. Heidbrink, C. M. Muscatello, R. Nazikian, M. A. Van Zeeland, and Y. B. Zhu, Rev. Sci. Instrum. **81**, 10D305 (2010).

[46] D. Darrow, J. Burby, M. Jokubaitis, and R. Nora, "Measurements and modeling of prompt loss of neutral beam ions from NSTX", the *52nd Annual Meeting of the APS Division of Plasma Physics, Chicago, Illinois, November 8–12* (2010).

[47] J. L. Terry, J. A. Snipes, and C. Kurz, Rev. Sci. Instrum. **66**, 555 (1995).

[48] S. Shiraiwa, O. Meneghini, R. Parker, G. Wallace, J. Wilson, I. Faust, C. Lau, R. Mumgaard, S. Scott, S. Wukitch, W. Beck, J. Doody, J. Irby, P. MacGibbon, D. Johnson, A. Kanojia, P. Koert, D. Terry, R. Vieira, and Alcator C-Mod team, Nucl. Fusion **51**, 103024 (2011).

[49] V. Petrzilka, V. Fuchs, J. Gunn, N. Fedorczak, A. Ekedahl, M. Goniche, J. Hillairet, and P. Pavlo, Plasma Phys. Controlled Fusion **53**, 054016 (2011).

[50] A. Cavallo, R. C. Cutler, and M. P. McCarthy, Rev. Sci. Instrum. **59**, 889 (1988).

[51] C. L. Fiore and R. L. Boivin, Rev. Sci. Instrum. **66**, 945 (1995).

[52] J. H. Irby, E. S. Marmar, E. Sevillano, and S. M. Wolfe, Rev. Sci. Instrum. **59**, 1568 (1988).

[53] V. Tang, J. Liptac, R. R. Parker, P. T. Bonoli, C. L. Fiore, R. S. Granetz, J. H. Irby, Y. Lin, S. J. Wukitch, J. A. Frenje, R. Leiter, S. Mcduffee, and R. D. Petrasso (Alcator C-Mod Team), Rev. Sci. Instrum. **77**, 083501 (2006).

[54] D. C. Pace, R. I. Pinsker, W. W. Heidbrink, R. K. Fisher, M. A. Van Zeeland, M. E. Austin, G. R. McKee, and M. García-Muñoz, Nucl. Fusion **52**, 063019 (2012).

[55] M. Garrett and S. Wukitch, "Mitigation of radio frequency sheaths through magnetic field-aligned ICRF antenna design," Fusion Eng. Des. (in press).

[56] D. Whyte, A. Hubbard, J. Hughes, B. Lipschultz, J. Rice, E. Marmar, M. Greenwald, I. Cziegler, A. Dominguez, T. Golfinopoulos, N. Howard, L. Lin, R. McDermott, M. Porkolab, M. Reinke, J. Terry, N. Tsujii, S. Wolfe, S. Wukitch, Y. Lin, and Alcator C-Mod Team, Nucl. Fusion **50**, 105005 (2010).

[57] W. W. Heidbrink, M. E. Austin, R. K. Fisher, M. García-Muñoz, G. Matsunaga, G. R. McKee, R. A. Moyer, C. M. Muscatello, M. Okabayashi, D. C. Pace, K. Shinohara, W. M. Solomon, E. J. Strait, M. A. V. Zeeland, and Y. B. Zhu, Plasma Phys. Controlled Fusion **53**, 085028 (2011).